BIOCHEMISTRY
including biophysical chemistry & molecular biology

Article

pubs.acs.org/biochemistry

Influence of 63Ser Phosphorylation and Dephosphorylation on the Structure of the Stathmin Helical Nucleation Sequence: A Molecular Dynamics Study

John H. Missimer,[†] Michel O. Steinmetz,[†] Wilfred F. van Gunsteren,[‡] and Jožica Dolenc*[,‡,§]

[†]Biomolecular Research, Paul Scherrer Institute, 5232 Villigen, Switzerland

[‡]Laboratory of Physical Chemistry, ETH, Swiss Federal Institute of Technology, 8093 Zürich, Switzerland

[§]Faculty of Chemistry and Chemical Technology, University of Ljubljana, 1000 Ljubljana, Slovenia

Supporting Information

ABSTRACT: Phosphorylation is an important mechanism regulating protein−protein interactions involving intrinsically disordered protein regions. Stathmin, an archetypical example of an intrinsically disordered protein, is a key regulator of microtubule dynamics in which phosphorylation of 63Ser within the helical nucleation sequence strongly down-regulates the tubulin binding and microtubule destabilizing activities of the protein. Experimental studies on a peptide encompassing the 19-residue helical nucleation sequence of stathmin (residues 55−73) indicate that phosphorylation of 63Ser destabilizes the peptide's secondary structure by disrupting the salt bridges supporting its helical conformation. In order to investigate this hypothesis at atomic resolution, we performed molecular dynamics simulations of nonphosphorylated and phosphorylated stathmin-[55−73] at room temperature and pressure, neutral pH, and explicit solvation using the recently released GROMOS force field 54A7. In the simulations of nonphosphorylated stathmin-[55−73] emerged salt bridges associated with helical configurations. In the simulations of 63Ser phosphorylated stathmin-[55−73] these configurations dispersed and were replaced by a proliferation of salt bridges yielding disordered configurations. The transformation of the salt bridges was accompanied by emergence of numerous interactions between main and side chains, involving notably the oxygen atoms of the phosphorylated 63Ser. The loss of helical structure induced by phosphorylation is reversible, however, as a final simulation showed. The results extend the hypothesis of salt bridge derangement suggested by experimental observations of the stathmin nucleation sequence, providing new insights into regulation of intrinsically disordered protein systems mediated by phosphorylation.

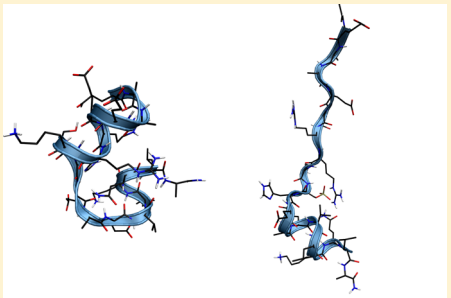

Intrinsically disordered proteins play important roles in many cellular processes including cell cycle control, signal transduction, and transcriptional regulation reviewed in ref 1. Post-translational regulation, effected, for example, by phosphorylation, is a widespread mechanism that modulates protein−protein interactions involving intrinsically disordered protein regions.[2]

The regulatory nature of phosphorylation has motivated several classical molecular dynamics simulations and quantum-mechanical/molecular-mechanical (QM/MM) calculations. Most of these deal with the effects of phosphorylation on loop stability and interactions among domains.[3−10] Two recent papers study the disorder-to-order transition induced by phosphorylation of serine in the 25-residue α-helical N-terminal phosphorylation domain of smooth muscle myosin.[11,12]

An example of an intrinsically disordered protein in which phosphorylation mediates regulation is stathmin, a key regulator of microtubule dynamics.[13,14] Its C-terminal domain, comprising about 140 amino acid residues, populates an ensemble of transient helical conformations that are nucleated from a distinct region spanning residues 55−73.[15] In contrast, the N-terminal domain, about 40 amino acid residues long, is devoid of stable tertiary structure in isolation. Upon binding of stathmin to two tubulin subunits, however, the N terminus folds into a β-hairpin, and the C-terminal helical domain becomes stabilized.[16] In vivo, the activity of stathmin is down-regulated by post-translational phosphorylation on four serine residues, 16Ser, 25Ser, 38Ser, and 63Ser.[17,18] Notably, phosphorylation of 63Ser within the helical nucleation sequence 55−73 of stathmin, denoted stathmin-[55−73], strongly down-regulates the tubulin binding and microtubule destabilizing activities of the protein.[15,17−20] Experimental studies, including circular dichroism and nuclear magnetic resonance spectroscopy, on a peptide encompassing the 19-residue helical nucleation sequence of stathmin indicate that phosphorylation of 63Ser destabilizes the helix nucleation sequence by disrupting the salt bridges supporting the helical

Received: July 2, 2012
Revised: September 13, 2012
Published: September 14, 2012

Table 1. Summary of Stathmin-[55−73] Simulations

designation	description			
	64His protonation	63Ser phosphorylation	temp [K]	Glu protonation
HE_300	NE		300	
HD_300	ND		300	
HE_P_300	NE	phosphorylated	300	
HD_P_300	ND	phosphorylated	300	
HE_278	NE		278	
HD_278	ND		278	
HE_P_278	NE	phosphorylated	278	
HD_P_278	ND	phosphorylated	278	
HE_300_65E	NE		300	65Glu
HE_300_67E	NE		300	67Glu
HE_P_300_67E	NE	phosphorylated	300	67Glu
HE_300_65E_67E	NE		300	65Glu, 67Glu
HH_300	ND, NE		300	
HH_300_67E	ND, NE		300	67Glu
HE_300_dP[a]	NE		300	

[a]Starting configuration is the final configuration of simulation HE_P_300.

structure and, as a consequence, the tubulin binding properties of stathmin.[15]

In order to investigate this hypothesis at atomic resolution, we have performed molecular dynamics simulations of stathmin-[55−73] in solution at room temperature and pressure, neutral pH, and explicit solvation using the recently released GROMOS force field 54A7.[21] Starting with the helical nucleation sequence derived from the observed X-ray crystal structure of stathmin bound to tubulin,[22] we simulated nonphosphorylated and phosphorylated forms of stathmin-[55−73] for 100 ns. The simulations performed in this study are summarized in Table 1.

In the initial simulation of nonphosphorylated stathmin-[55−73] a kink emerged in the midst of the predominantly helical peptide that was not consistent with measured chemical shifts. We explored possible sources of this kink in numerous simulations of the peptide at two temperatures and numerous protonation states. In only one case did the kink not develop, yielding chemical shifts consistent with experiment.

While the appearance of the kink provided the motivation for the numerous simulations, the effect of phosphorylation is similar in all cases: the salt bridges associated with helical configurations dispersed, replaced by a proliferation of salt bridges yielding disordered configurations. The transformation of the salt bridges was accompanied by disappearance of the hydrogen bonds associated with helical configurations and emergence of numerous interactions between main and side chains, involving notably the oxygen atoms of the phosphorylated 63Ser. The loss of order induced by phosphorylation is reversible, however, as a final simulation showed. When the phosphate group is replaced by a hydrogen atom, the salt bridges and hydrogen bonds associated with helical configurations reappear within 150 ns and the peptide resumes configurations found in the simulations of nonphosphorylated stathmin-[55−73].

Thus, the simulations confirm the disruption of salt bridges associated with helical configurations in phosphorylated stathmin-[55−73] suggested by experiment and, further, indicate that proliferation of salt bridges accompanies the disruption. The configurations in phosphorylated stathmin-[55−73] are disordered, but dephosphorylation quickly restores the helical configurations of nonphosphorylated peptide.

METHODS

Simulations. The molecular dynamics simulations reported here were carried out using the GROMOS biomolecular simulation package[23−25] and the 54A7 GROMOS force-field parameter sets.[21] Force-field parameters for phosphorylated Ser were selected in analogy to existing parameters in the GROMOS 54A7 force field and are reported in Figure S1 and in Tables S1−S5 of the Supporting Information. For the phosphate group an overall charge of $-2e$ has been used. The 19-residue α-helical nucleation sequence of stathmin comprises the sequence Ac-55Glu-56Ala-57Ala-58Glu-59Glu-60Arg-61Arg-62Lys-63Ser-64His-65Glu-66Ala-67Glu-68Val-69Leu-70Lys-71Gln-72Leu-73Ala-NH2. In accordance with the measurements being performed at neutral pH, the Arg and Lys side chains were protonated with charge $+e$. The His residue was neutrally charged with a hydrogen at either NE (HisE) or ND (HisD) since both states are likely to be present at neutral pH. Six of the 15 reported simulations assumed protonated 64His with charge $+e$ or protonated neutral 65Glu or 67Glu side chains. All simulations summarized in Table 1 were performed with explicit solvation. Starting coordinates for MD simulations of both phosphorylated and nonphosphorylated stathmin-[55−73] were derived from the X-ray crystal structure of the nonphosphorylated peptide bound to tubulin, stathmin-[1−141].[22] The final coordinates of the simulation of phosphorylated stathmin-[55−73] at 300 K, HE_P_300, served as the starting coordinates for the simulation of dephosphorylated stathmin-[55−73], HE_300_dP.

The simulations were performed using periodic boundary conditions. After steepest descent energy minimization, the structure was solvated in a rectangular box of ∼3400 pre-equilibrated simple point charge (SPC) water molecules[26] with a minimal solute-to-wall distance of 1.0 nm. The system was relaxed by performing a steepest-descent energy minimization with harmonic positional restraints on all solute atoms (force constant 2.5×10^4 kJ mol^{-1} nm^{-2}) followed by a 100 ps long equilibration, in which the positional restraints were gradually released reducing the force constant to 0.0 kJ mol^{-1} nm^{-2} and the temperature was raised from 60 K to 278 or 300 K. The

dx.doi.org/10.1021/bi300885y | Biochemistry 2012, 51, 8455−8463

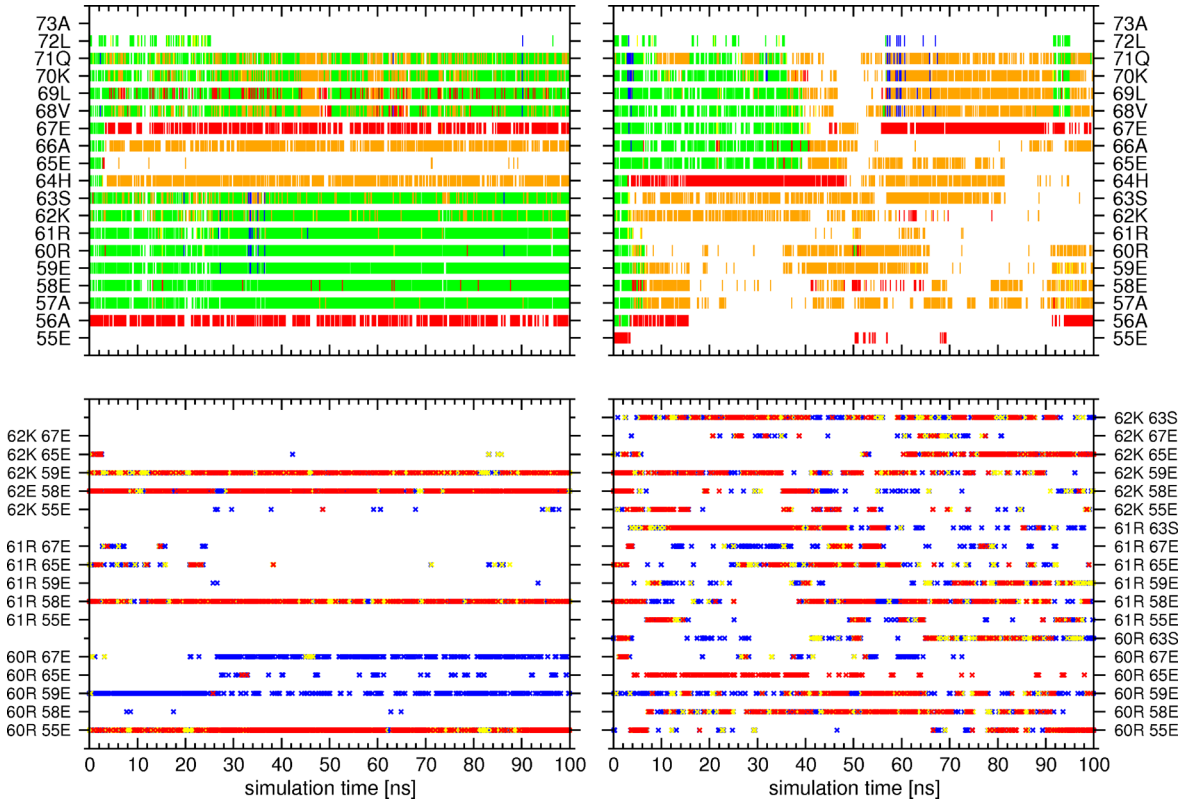

Figure 1. Time evolutions of secondary structures (upper panels) and salt bridges (lower panels) yielded by simulations HE_300 and HE_P_300 in the case of nonphosphorylated (left) and phosphorylated (right) 63Ser. In the graphs of secondary structures, green indicates α-helix, red turn, orange bend, yellow 3_{10} helix, and blue π-helix; to reduce overlap configurations are depicted every 100 ps. In graphs of salt bridges, the colors indicate the fraction of the total number of possible contacts occupied in a specific time interval: blue indicates less than 33%, yellow between 33% and 66%, and red greater than 66%.

initial atomic velocities were taken from a Maxwell distribution at 60 K. The equations of motion were integrated using the leapfrog algorithm with a time step of 2 fs. Center-of-mass motion was stopped every 2 ps. Bond lengths of the peptide and the geometry of the water molecules were constrained by applying the SHAKE algorithm[27] with a relative geometric tolerance of 10^{-4}. The temperature and pressure were maintained at 278 or 300 K and 1 atm using the Berendsen thermostat with a coupling time $\tau_T = 0.1$ ps and barostat with a coupling time $\tau_P = 0.5$ ps and an isothermal compressibility[28] of 4.575×10^{-4} (kJ mol^{-1} nm^{-3})$^{-1}$. A reaction-field approach was used to treat the electrostatics employing a triple-range cutoff scheme, with cutoffs of 0.8 and 1.4 nm and a dielectric permittivity[29] of 66.6. The pair list was updated every five steps. All simulations were performed for 100 ns except for HE_300_dP, which was extended to 150 ns.

Analysis. The trajectory configurations were saved every 1 ps. The secondary structure assignment was done with the program DSSP, based on the Kabsch−Sander rules.[30] Occurrences of hydrogen bonds and salt bridges were calculated from the 100 000 saved trajectory configurations. Hydrogen bonds were defined by a minimum donor−H-acceptor angle of 135° and a maximum H-acceptor distance of 0.25 nm. Similarly, salt bridges were defined by a maximum distance of 0.6 nm between the partially charged protons HE and HH of 60Arg or 61Arg or HZ of 62Lys or 70Lys and oxygens OE of 55Glu, 58Glu, 59Glu, 65Glu, and 67Glu or OP of phosphorylated 63Ser. Thus, the number of possible Arg-Glu salt bridges is 10, of Lys-Glu salt bridges 6, of Arg-Ser salt bridges 15, and of Lys-Ser salt bridges 9; these numbers determine the color codes in the graphs depicting the time courses of the salt bridges. Average chemical shifts for Cα of the peptide backbone were calculated from a set of structures taken at 100 ps intervals using the program[31] SHIFTX2 and are reported as a difference between the calculated average chemical shift of the residue and the respective reference random coil chemical shift value. Reference random coil chemical shift values were taken from ref 15 and are listed in the Table S6 of the Supporting Information. A cluster analysis of peptide conformations was performed on every fifth frame of the simulated trajectories, i.e., at 5 ps intervals. The clustering algorithm, which uses the atom-positional rmsd as similarity criterion, has been described in previous studies of peptide dynamics.[32] For this analysis, it performed a translational superposition of centers of mass and a rotational least-squares fit for every pair of configurations using backbone atoms CA, N, and C, excluding the terminal residues 55 and 73, and calculated the corresponding atom-positional rmsd for the same set of atoms. The cluster criterion was a backbone atom-positional rmsd of less than 0.2 nm. For visual analysis the VMD program was used.[33]

RESULTS

As evidenced by the analysis of secondary structure of simulation HE_300, shown in the upper panels of Figure 1, the nonphosphorylated stathmin α-helical nucleation sequence retained full α-helical structure only in the first few nanoseconds. After that, 65Glu evidences no defined secondary

dx.doi.org/10.1021/bi300885y | Biochemistry 2012, 51, 8455−8463

structure and the adjacent residues show a bend; the N-terminal residues between 57 and 63 maintain α-helical structure whereas the C-terminal residues between 68 and 72 fluctuate between α-helix and bend. The topology of the dominant structure shown in Figure 2 shows a kink comprising

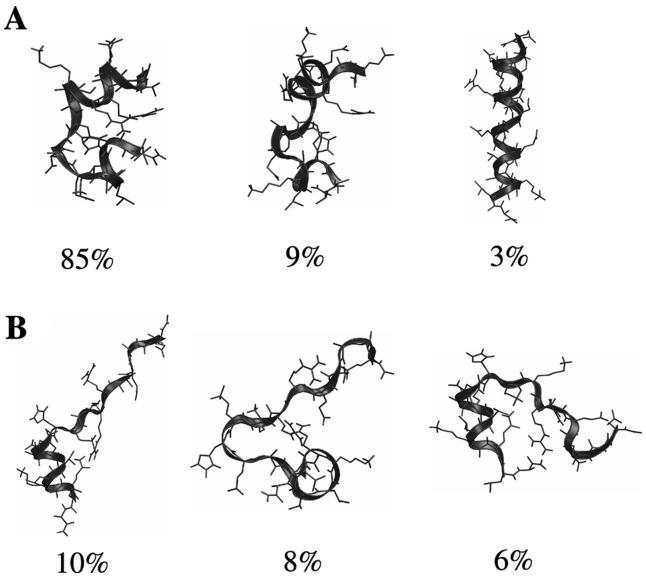

Figure 2. Central members of the three dominant clusters derived from the trajectories of HE_300 and HE_P_300 are shown for nonphosphorylated (upper panels) and phosphorylated (lower panels) 63Ser. The central member structures correspond to simulation times 63, 20, and 5 ns for HE_300 and to simulation times 24, 70, and 12 ns for HE_P_300.

the residues 64−66; this deformation of the helical configuration is also evident in the chemical shifts shown in Figure 3. Suspecting the origin might lie in our choice of the 64His residue protonated at NE or of the simulation temperature, 300 K, we performed additional simulations at the temperature 278 K, at which chemical shift measurements were made as well as simulations of the 64His residue protonated at ND at both temperatures.

Figure 1 indicates also that phosphorylation of the stathmin nucleation sequence simulated in HE_P_300 causes pronounced changes in the secondary structure of the stathmin nucleation sequence. The initial α-helical structure again remains stable only during the first nanoseconds. Afterward, the C-terminal residues between 65 and 72 maintain the α-helical structure until 40 ns, whereas the N-terminal residues between 55 and 64 undergo transitions to turns or loose particular secondary structure completely. After 40 ns the α-helix of the C-terminal residues transforms predominantly to bends interrupted by brief interludes of α- or π-helices. Thus, phosphorylation yields a markedly less ordered secondary structure, as suggested by Figures 1−3.

The disorder associated with phosphorylation is also evident in the analysis of salt bridges shown in the lower panels of Figure 1. The nonphosphorylated nucleation sequence is dominated throughout the simulation by four sets of salt bridges: contacts between 55Glu and 60Arg, between 58Glu and 61Arg, between 58Glu and 62Lys, and between 59Glu and 62Lys. Less important are contacts between 59Glu and 60Arg; contacts between 60Arg and 65Glu or 67Glu appear with the bends at the C-terminal end. The phosphorylated nucleation sequence indicates a proliferation of salt bridges distributed nonuniformly over all possible contacts with no apparent dominant contacts. Quantitatively, the phosphorylated nucleation sequence exhibits 70% more contacts than the nonphosphorylated sequence.

Analyses of secondary structure of trajectories of HD_300, shown in the upper left panels of Figure S2, and of simulations HE_278 and HD_278, shown in Figures S3 and S4, exhibit similar patterns. A break in the secondary structures of the

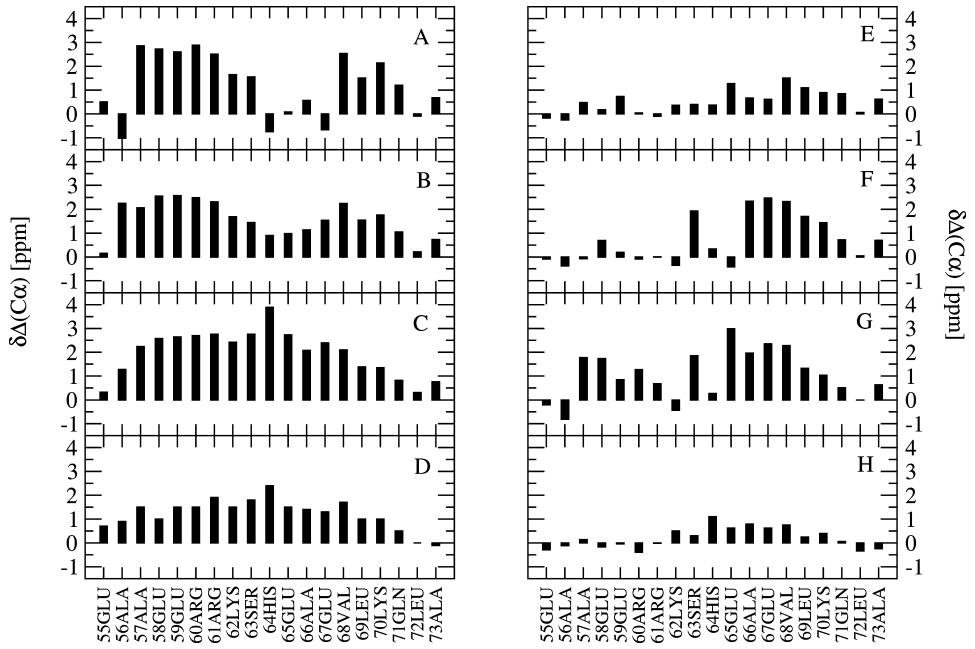

Figure 3. Average Cα chemical shifts for each residue of stathmin-[55−73] calculated for the simulations HE_300 and HE_P_300 (upper row), HD_300 and HD_P_300 (second row), and HE_300_67E and HE_P_300_67E with protonated 67Glu (third row) compared with the experimental shifts (lowest row) for nonphosphorylated (left column) and phosphorylated (right column) stathmin nucleation sequence.

dx.doi.org/10.1021/bi300885y | *Biochemistry* 2012, 51, 8455−8463

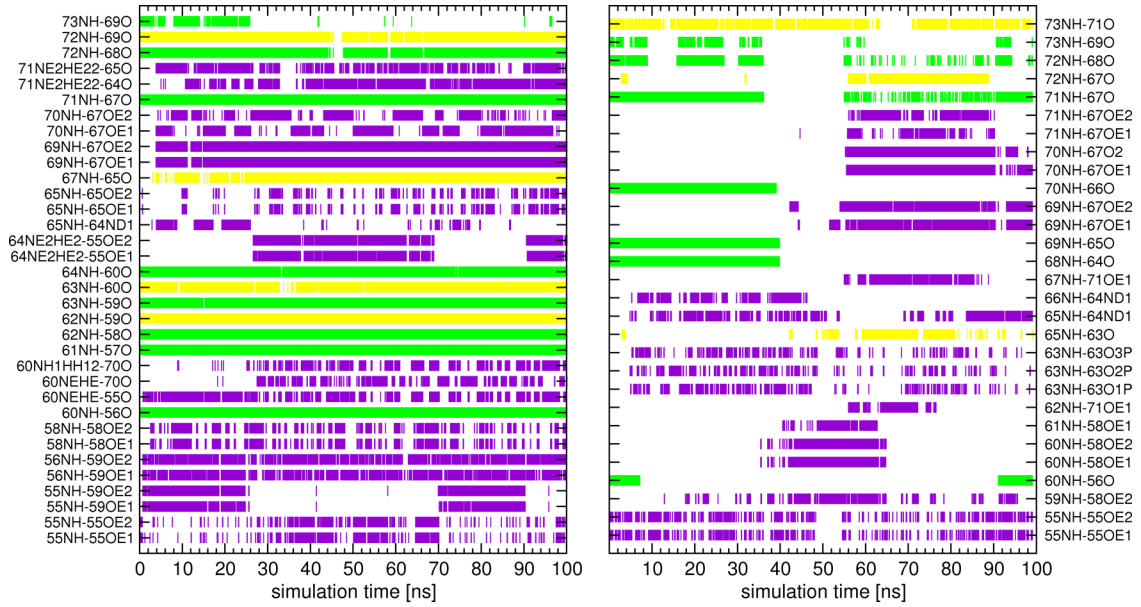

Figure 4. Simulated time evolutions of hydrogen bonds for nonphosphorylated (left) and phosphorylated (right) stathmin nucleation sequence for simulations HE_300 and HE_P_300. Green denotes main chain hydrogen bonds between residues i,i-4; yellow, those between residues i,i-3 or i,i-2; and blue, those between i,i-5. Violet denotes hydrogen bonds between main and side chains and indigo those between side chains. Only bonds exceeding 10% occurrence are listed.

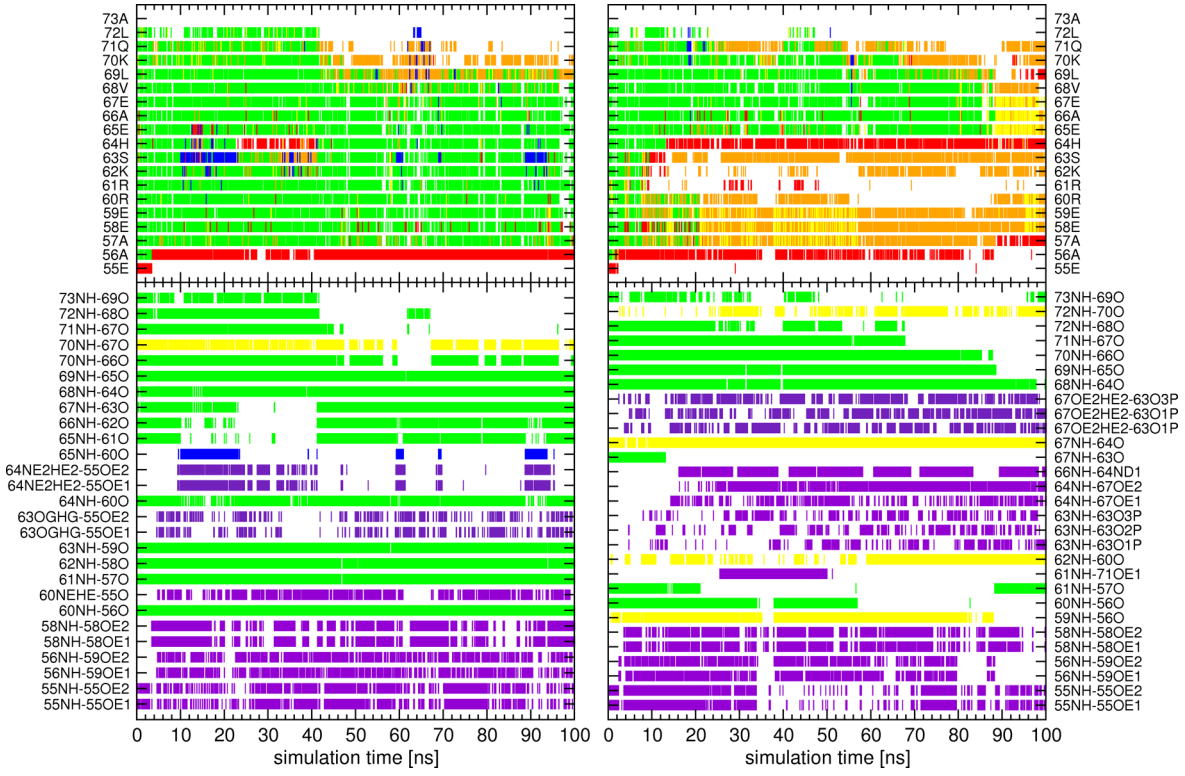

Figure 5. Simulated time evolution of secondary structure (upper panels) and hydrogen bonds (lower panels) for nonphosphorylated (left panels) and phosphorylated (right panels) stathmin nucleation sequence with protonated 67Glu for simulations HE_300_67E and HE_P_300_67E. The color coding is identical to that of Figures 1 and 4.

nonphosphorylated nucleation sequence at 65Glu develops between 10 and 40 ns after the beginning of the simulations, although its appearance differs in each case. In the trajectories of HD_300, the break is characterized by lack of structure or bend at 65Glu and 64His and turn or bend at 66Ala; in trajectories of HE_278 and HD_278, by turns at 65Glu and bends at 64His. In trajectories of HD_300 and HD_278, the C-terminal residues between 68 and 72 evolve into bends or loose secondary structure completely, whereas trajectory of HE_278 maintain α-helical structure. In every case, the break is the signature of the kinks shown in Figures S5−S7 and confirmed by the chemical shifts of Figure S8. In the case of the

dx.doi.org/10.1021/bi300885y | *Biochemistry* 2012, 51, 8455−8463

phosphorylated nucleation sequence, the secondary structures of trajectories of HD_P_300, HD_P_278 and HE_P_278 show a pattern similar to that of HE_P_300; the N-terminal residues evolve predominantly to bends, turns, or loose secondary structure completely. However, the residue at which the disorder occurs varies. Whereas the critical residue in the trajectory of HE_P_300 is 64His, in the trajectory of HE_P_278, it is 67Glu; in the trajectory of HD_P_300, it is 65Glu; and in the trajectory of HD_P_278, it is 61Arg. In all three cases, especially in that of HD_P_278, the residues above the critical residue maintain α-helical structure to a greater extent than in the case of HE_P_300.

Analyses of the salt bridges shown in the lower panels of Figures S2−S4 exhibit the same increase in contacts of the phosphorylated nucleation sequence relative to the non-phosphorylated sequence. In both His variants at both temperatures, contacts between 58Glu or 59Glu and 62Lys were most frequent in the nonphosphorylated peptide, while contacts between 58Glu and 61Arg, between 59Glu and 60Arg, and between 55Glu and 60Arg appear also in both His variants at both temperatures, but with varying relative frequencies.

Analysis of the hydrogen bonds shown in Figure 4 and Figures S9−S11 reveals that adjacent to the kink at both terminal ends most hydrogen bonds associated with α-helices, i,i-4 or i,i-3, persist during the entire simulation. The analysis also exhibits a common feature involving the two residues 65Glu and 67Glu: hydrogen bonds between the side chains of these residues and their own backbone or those of neighboring residues appear at about the same time as the kink pattern in the secondary structure.

This pattern and the hypothesis that the local environment might be substantially more acidic than indicated by neutral pH stimulated us to perform additional simulations with modified protonation states of 64His, 65Glu, and 67Glu. Remarkably, of the simulations HE_300_65E, HE_300_67E, HE_300_65E_67E, HH_300, and HH_300_67E, only HE_300_67E failed to develop a kink. Those that evidenced a kink showed the pattern of hydrogen bonds between the side chains of 65Glu or 67Glu and their own backbone or those of neighboring residues seen in the simulations of stathmin-[55−73] with unprotonated residues discussed above. The secondary structure of the simulation exhibiting no kink, HE_300_67E, shown in Figure 5, evidences noticeable admixtures of π- and 3_{10}-helices in the middle and at the C-terminal end of the peptide to which the chemical shifts shown in Figure 3 are not sensitive. Concurrent with the appearance of π-helices in the middle is formation of a main-chain i,i-5 hydrogen bond between 65Glu and 60Arg and, remarkably, side-chain hydrogen bonds between 64His and 55Glu. The latter bonds persist between 20 and 40 ns when the main-chain hydrogen bond and the i,i-4 bonds between 65Glu and 61Arg, 66Ala and 62Lys, and 67Glu and 63Ser dissolve, accompanied by secondary structure fluctuating between turn, π- and 3_{10}-helices. At the end of this period, the i,i-4 bonds reappear, but the three i,i-4 bonds at the C-terminal end dissolve. The simulation of the corresponding phosphorylated peptide, HE_P_300_67E, yielded the secondary structure and hydrogen bonds also shown in Figure 5; these resemble the original four simulations of the phosphorylated peptide with the border between helical and nonhelical secondary structure at 64His. The salt bridges, not shown, exhibit a proliferation similar to the original four simulations.

The proliferation of salt bridges in all simulations of phosphorylated stathmin-[55−73] suggested a study of dephosphorylation. Beginning with the final configuration of the simulation HE_P_300 as starting structure, the phosphate group was replaced by a hydrogen yielding a nonphosphorylated stathmin-[55−73] with the configuration of the phosphorylated stathmin-[55−73]. The trajectory of this nonphosphorylated peptide evidences in the secondary structure shown in Figure 6 the emergence of α-helical

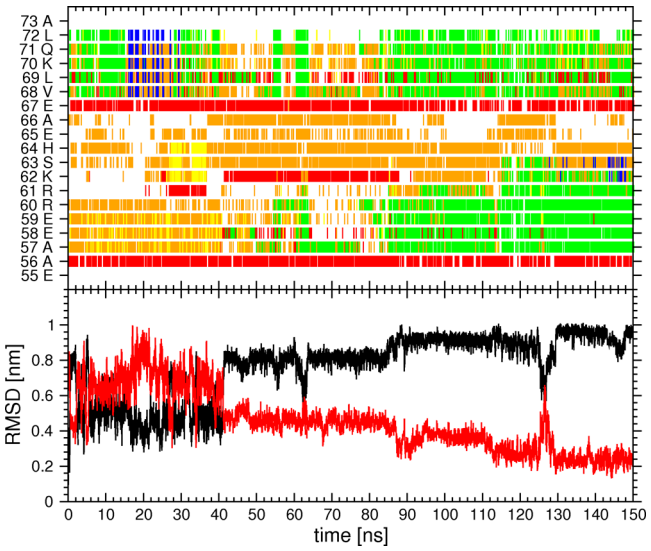

Figure 6. In the lower panel are graphed for the simulation HE_300_dP the time evolutions of root-mean-squared deviations from the final configuration of the simulation HE_P_300 of phosphorylated stathmin nucleation sequence, in which the phosphate group has been replaced by a hydrogen atom (black) and from the final configuration of the simulation HE_300 of nonphosphorylated stathmin nucleation sequence (red). The time evolution of the corresponding secondary structure of the dephosphorylated peptide is shown in the upper panel. The color coding is identical to that of Figure 1.

structure first in the five C-terminal residues adjacent to 67Glu and then in the four N-terminal residues adjacent to 61Arg, suggesting convergence to the secondary structure observed in the simulation HE_300. The convergence is supported by the root-mean-squared deviations from the final configuration of HE_300, represented by the red curve in the lower panel of the Figure 6, which decreases to less than 0.4 nm after 100 ns of simulation. The black curve shows the deviation from the initial structure, the final configuration of HE_P_300. Analyses of salt bridges and hydrogen bonds shown in Figure 7 also confirm the formation of the dominantly α-helical structure observed in HE_300. The number of salt bridges decreases markedly, and the four most prominent in HE_300, associated with helical structure in the N-terminal end, dominate. In addition, the three corresponding i,i-4 hydrogen bonds are formed.

DISCUSSION AND CONCLUSIONS

The structural mechanism of reversible protein phosphorylation, a process frequently used in cells to regulate the activity of disordered proteins, is only poorly understood. Stathmin is an archetypal example of an intrinsically disordered phosphoprotein that assumes structure upon interacting with its binding-

dx.doi.org/10.1021/bi300885y | *Biochemistry* 2012, 51, 8455−8463

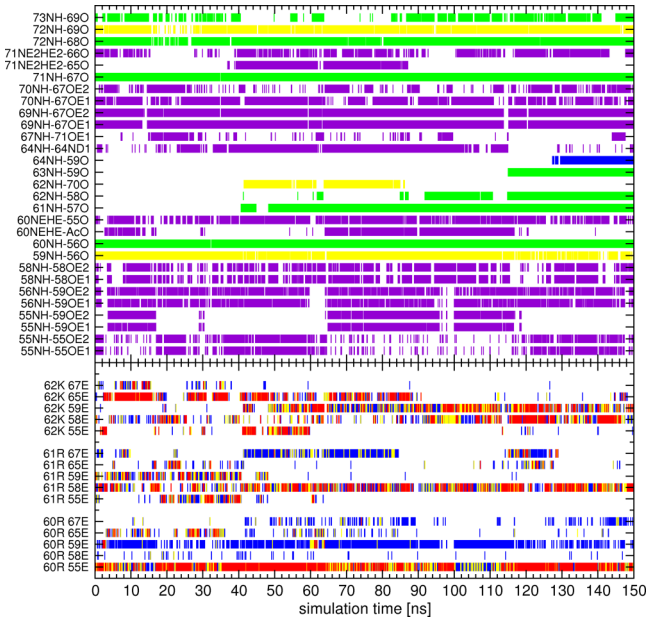

Figure 7. Simulated time evolution of hydrogen bonds (upper panel) and salt bridges (lower panel) found in simulation HE_300_dP of dephosphorylated stathmin nucleation sequence. The color coding is identical to that of Figures 1 and 4.

partner tubulin (reviewed in ref 14). The helical nucleation sequence (residues 55−73) of stathmin triggers complex formation with tubulin, and phosphorylation of 63Ser in the middle of the sequence decreases its affinity for tubulin.[15,19] Thus, stathmin exemplifies a commonly used mechanism in which transient helix formation mediates interactions between an intrinsically disordered protein and its folded binding target.[34]

Consistent with experimental studies of the 19-residue helical nucleation sequence [55−73] of stathmin,[15] including circular dichroism and nuclear magnetic resonance spectral data and chemical shifts, our MD simulations reveal that phosphorylation of 63Ser disrupts the conformation of the helical nucleation sequence. On the residue level, the chemical shifts indicate helical configurations from residue 55 to 71 in the nonphosphorylated peptide, less helical configurations in the C-terminal end of the phosphorylated peptide, and none in the N-terminal end. The MD simulations reported above show a disruption of the salt bridges that accompany α-helical structure; the clear pattern of salt bridges evident in four simulations of the nonphosphorylated stathmin nucleation peptide with 64His protonated at ND or NE at two temperatures disperses in simulations of the corresponding phosphorylated peptide. All four of the latter simulations show in secondary structure and chemical shifts complete loss of helical structure at the N-terminal end, and three simulations evidence some helical structure at the C-terminal end. The structural disorder of the phosphorylated peptide is accompanied by a proliferation of salt bridges not expected from the simple addition of the phosphate group.

In conflict with the experimental chemical shift data is the occurrence of a kink in the middle of the peptide in four simulations of the nonphosphorylated peptide. Noting that its appearance was always associated with the emergence of hydrogen bonds between the side chains of 65Glu or 67Glu with their own backbones or those of neighboring residues, we performed simulations of the nonphosphorylated peptide in which one or both glutamate residues were protonated. Suspecting that these two negatively charged side chains could provide a local acidic environment, we also performed simulations in which 64His was doubly protonated. Of the five simulations, only the one in which 67Glu was protonated yielded no kink. However, the trajectory of this simulation does evidence short-lived fluctuations of bends, turns, and π-helices in the kink region and unraveling at the C-terminal end, indicating marginal stability. In the context of the other simulations, this result suggests that the kink is a subtle artifact of the partial charges of atoms of negatively charged side chains in the force field or of the simplified model of implicit fixed pH in MD simulations. In contrast to nonpolar and polar residues, the force-field parameters for charged residues have not been subjected to thermodynamic tests of validation, and the water model does not include hydronium ions which could affect the local environment.

An important aspect of the simulations with protonated 67Glu is that simulations of the phosphorylated peptide showed a pattern of secondary structure, hydrogen bonds, and salt bridges similar to that of the original four simulations, indicating that the loss of order associated with phosphorylation of the peptide is associated with a proliferation of salt bridges, not with their complete dissolution. This proliferation enables the peptide to resume order rapidly when dephosphorylation takes place, as shown by the simulation starting from the final configuration of the phosphorylated peptide in which the phosphate group was replaced by a hydrogen. These results extend the hypothesis of salt bridge derangement based on experimental observations of the stathmin nucleation sequence, providing new insights into regulation of an intrinsically disordered protein system mediated by phosphorylation. They support at atomistic resolution the hypothesis that the phosphorylation-induced disruption of helical structure down-regulates the affinity of stathmin for tubulin, as suggested by the observation that in the tubulin−stathmin complex the side chain of Ser63 is located remote from the protein−protein interface, pointing into the solution (reviewed in ref 14). The alternative hypothesis, that the down-regulation is a direct effect at the protein−protein interface, appears unfounded. Thus, the simulations illustrate that the perturbation of local secondary structure by post-translational phosphorylation represents an attractive mechanism for fine-tuning the association−dissociation properties of assemblies involving intrinsically disordered protein complexes.

■ ASSOCIATED CONTENT

Supporting Information

Tables S1−S5: force field parameters for phosphorylated Ser; Table S6: random coil Cα chemical shifts used in this work; Figure S1: chemical structure of phosphorylated serine; Figures S2−S4: time evolution of secondary structure and salt bridges for simulations HD_300, HE_278, and HD_278; Figures S5−S7: central members of the three dominant clusters for the same three simulations; Figure S8: calculated chemical shifts for each residue in the simulations of HE_278, HD_278, HE_P_278, and HD_P_278 compared with the corresponding experimental shifts; Figures S9−S11: time evolution of hydrogen bonds for the simulations HD_300, HE_278, and HD_278; Figure S12: central members of the three dominant clusters for the simulations HE_300_67E and

dx.doi.org/10.1021/bi300885y | Biochemistry 2012, 51, 8455−8463

HE_P_300_67E. This material is available free of charge via the Internet at http://pubs.acs.org.

AUTHOR INFORMATION

Corresponding Author

*E-mail jozi@igc.phys.chem.ethz.ch; Tel +41 44 632 42 39.

Author Contributions

The manuscript was written through contributions of all authors. All authors have given approval to the final version of the manuscript.

Funding

This work was financially supported by the National Center of Competence in Research (NCCR) in Structural Biology and by Grant 200020-137827 of the Swiss National Science Foundation and by Grant 228076 of the European Research Council, which is gratefully acknowledged.

Notes

The authors declare no competing financial interest.

ACKNOWLEDGMENTS

The authors thank Daan Geerke and Zhixiong Lin for assistance in setting up preliminary simulations.

REFERENCES

(1) Dyson, H. J., and Wright, P. E. (2005) Intrinsically unstructured proteins and their functions. *Nat. Rev. Mol. Cell Biol. 6*, 197−208.

(2) Iakoucheva, L. M., Radivojac, P., Brown, C. J., O'Connor, T. R., Sikes, J. G., Obradovic, Z., and Dunker, A. K. (2004) The importance of intrinsic disorder for protein phosphorylation. *Nucleic Acids Res. 32*, 1037−1049.

(3) Diaz, N., and Field, M. J. (2004) Insights into the phosphoryl-transfer mechanism of cAMP-dependent protein kinase from quantum chemical calculations and molecular dynamics simulations. *J. Am. Chem. Soc. 126*, 529−542.

(4) Hamelberg, D., Shen, T., and McCammon, J. A. (2005) Phosphorylation effects on cis/trans isomerization and the backbone conformation of serine-proline motifs: Accelerated molecular dynamics analysis. *J. Am. Chem. Soc. 127*, 1969−1974.

(5) Metcalfe, E. E., Traaseth, N. J., and Veglia, G. (2005) Serine 16 phosphorylation induces an order-to-disorder transition in monomeric phospholamban. *Biochemistry 44*, 4386−4396.

(6) Cheng, Y. H., Zhang, Y. K., and McCammon, J. A. (2006) How does activation loop phosphorylation modulate catalytic activity in the cAMP-dependent protein kinase: A theoretical study. *Protein Sci. 15*, 672−683.

(7) Groban, E. S., Narayanan, A., and Jacobson, M. P. (2006) Conformational changes in protein loops and helices induced by post-translational phosphorylation. *PLoS Comput. Biol. 2*, 238−250.

(8) Jin, H. X., Wu, T. X., Jiang, Y. J., Zou, J. W., Zhuang, S. L., Mao, X., and Yu, Q. S. (2007) Role of phosphorylated Thr-197 in the catalytic subunit of cAMP-dependent protein kinase. *J. Mol. Struct.: THEOCHEM 805*, 9−15.

(9) Suenaga, A., Hatakeyama, M., Kiyatkin, A. B., Radhakrishnan, R., Taiji, M., and Kholodenko, B. N. (2009) Molecular dynamics simulations reveal that Tyr-317 phosphorylation reduces Shc binding affinity for phosphotyrosyl residues of epidermal growth factor receptor. *Biophys. J. 96*, 2278−2288.

(10) Narayanan, A., LeClaire, L. L., Barber, D. L., and Jacobson, M. P. (2011) Phosphorylation of the Arp2 subunit relieves auto-inhibitory interactions for Arp2/3 complex activation. *PLoS Comput. Biol. 7*, e1002226 DOI: 10.1371/journal.pcbi.1002226.

(11) Espinoza-Fonseca, L. M., Kast, D., and Thomas, D. D. (2007) Molecular dynamics Simulations reveal a disorder-to-order transition on phosphorylation of smooth muscle myosin. *Biophys. J. 93*, 2083−2090.

(12) Kast, D., Espinoza-Fonseca, L. M., Yi, C., and Thomas, D. D. (2010) Phosphorylation-induced structural changes in smooth muscle myosin regulatory light chain. *Proc. Natl. Acad. Sci. U. S. A. 107*, 8207−8212.

(13) Steinmetz, M. O., Kammerer, R. A., Jahnke, W., Goldie, K. N., Lustig, A., and van Oostrum, J. (2000) Op18/stathmin caps a kinked protofilament-like tubulin tetramer. *EMBO J. 19*, 572−580.

(14) Steinmetz, M. O. (2007) Structure and thermodynamics of the tubulin-stathmin interaction. *J. Struct. Biol. 158*, 137−147.

(15) Steinmetz, M. O., Jahnke, W., Towbin, H., Garcia-Echeverria, C., Voshol, H., Müller, D., and van Oostrum, J. (2001) Phosphorylation disrupts the central helix in Op18/stathmin and suppresses binding to tubulin. *EMBO Rep. 2*, 505−510.

(16) Gigant, B., Wang, C. G., Ravelli, R. B. G., Roussi, F., Steinmetz, M. O., Curmi, P. A., Sobel, A., and Knossow, M. (2005) Structural basis for the regulation of tubulin by vinblastine. *Nature 435*, 519−522.

(17) Larsson, N., Marklund, U., Gradin, H. M., Brattsand, G., and Gullberg, M. (1997) Control of microtubule dynamics by oncoprotein 18: Dissection of the regulatory role of multisite phosphorylation during mitosis. *Mol. Cell. Biol. 17*, 5530−5539.

(18) Kuntziger, T., Gavet, O., Sobel, A., and Bornens, M. (2001) Differential effect of two stathmin/Op18 phosphorylation mutants on Xenopus embryo development. *J. Biol. Chem. 276*, 22979−22984.

(19) Honnappa, S., Jahnke, W., Seelig, J., and Steinmetz, M. O. (2006) Control of intrinsically disordered stathmin by multisite phosphorylation. *J. Biol. Chem. 281*, 16078−16083.

(20) Manna, T., Thrower, D. A., Honnappa, S., Steinmetz, M. O., and Wilson, L. (2009) Regulation of microtubule dynamic instability in vitro by differentially phosphorylated stathmin. *J. Biol. Chem. 284*, 15640−15649.

(21) Schmid, N., Eichenberger, A. P., Choutko, A., Riniker, S., Winger, M., Mark, A. E., and van Gunsteren, W. F. (2011) Definition and testing of the GROMOS force-field versions 54A7 and 54B7. *Eur. Biophys. J. Biophys. Lett. 40*, 843−856.

(22) Ravelli, R. B. G., Gigant, B., Curmi, P. A., Jourdain, I., Lachkar, S., Sobel, A., and Knossow, M. (2004) Insight into tubulin regulation from a complex with colchicine and a stathmin-like domain. *Nature 428*, 198−202.

(23) Eichenberger, A. P., Allison, J. R., Dolenc, J., Geerke, D. P., Horta, B. A. C., Meier, K., Oostenbrink, C., Schmid, N., Steiner, D., Wang, D. Q., and van Gunsteren, W. F. (2011) GROMOS++ software for the analysis of biomolecular simulation trajectories. *J. Chem. Theory Comput. 7*, 3379−3390.

(24) Kunz, A. P. E., Allison, J. R., Geerke, D. P., Horta, B. A. C., Hünenberger, P. H., Riniker, S., Schmid, N., and van Gunsteren, W. F. (2012) New functionalities in the GROMOS biomolecular simulation software. *J. Comput. Chem. 33*, 340−353.

(25) Schmid, N., Christ, C. D., Christen, M., Eichenberger, A. P., and van Gunsteren, W. F. (2012) Architecture, implementation and parallelisation of the GROMOS software for biomolecular simulation. *Comput. Phys. Commun. 183*, 890−903.

(26) Berendsen, H. J. C., Postma, J. P. M., van Gunsteren, W. F., and Hermans, J. (1981) Interaction models for water in relation to protein hydration, in *Intermolecular Forces* (Pullman, B., Ed.) pp 331−342, Reidel, Dordrecht, The Netherlands.

(27) Ryckaert, J. P., Ciccotti, G., and Berendsen, H. J. C. (1977) Numerical integration of cartesian equations of motion of a system with constraints: Molecular dynamics of N-alkanes. *J. Comput. Phys. 23*, 327−341.

(28) Berendsen, H. J. C., Postma, J. P. M., van Gunsteren, W. F., Dinola, A., and Haak, J. R. (1984) Molecular dynamics with coupling to an external bath. *J. Chem. Phys. 81*, 3684−3690.

(29) Glättli, A., Daura, X., and van Gunsteren, W. F. (2002) Derivation of an improved simple point charge model for liquid water: SPC/A and SPC/L. *J. Chem. Phys. 116*, 9811−9828.

(30) Kabsch, W., and Sander, C. (1983) Dictionary of protein secondary structure: Pattern recognition of hydrogen-bonded and geometrical features. *Biopolymers 22*, 2577−2637.

(31) Han, B., Liu, Y., Ginzinger, S., and Wishart, D. (2011) SHIFTX2: significantly improved protein chemical shift prediction. *J. Biomol. NMR 50*, 43−57.
(32) Daura, X., Mark, A. E., and van Gunsteren, W. F. (1998) Parametrization of aliphatic CHn united atoms of GROMOS96 force field. *J. Comput. Chem. 19*, 535−547.
(33) Humphrey, W., Dalke, A., and Schulten, K. (1996) VMD: Visual molecular dynamics. *J. Mol. Graphics 14*, 33−38.
(34) Wright, P. E., and Dyson, H. J. (1999) Intrinsically unstructured proteins: Re-assessing the protein structure-function paradigm. *J. Mol. Biol. 293*, 321−331.